A&A 656, L11 (2021)
https://doi.org/10.1051/0004-6361/202141009

Astronomy & Astrophysics
Special issue

Solar Orbiter First Results (Cruise Phase)

LETTER TO THE EDITOR

The long period of ^{3}He-rich solar energetic particles measured by Solar Orbiter 2020 November 17–23

R. Bučík[1], G. M. Mason[2], R. Gómez-Herrero[3], D. Lario[4], L. Balmaceda[4,5], N. V. Nitta[6], V. Krupař[4,7], N. Dresing[8,9], G. C. Ho[2], R. C. Allen[2], F. Carcaboso[3], J. Rodríguez-Pacheco[3], F. Schuller[10], A. Warmuth[10], R. F. Wimmer-Schweingruber[8], J. L. Freiherr von Forstner[8,11], G. B. Andrews[2], L. Berger[8], I. Cernuda[3], F. Espinosa Lara[3], W. J. Lees[2], C. Martín[8,12], D. Pacheco[8], M. Prieto[3], S. Sánchez-Prieto[3], C. E. Schlemm[2], H. Seifert[2], K. Tyagi[2,13], M. Maksimovic[14], A. Vecchio[14,15], A. Kollhoff[8], P. Kühl[8], Z.G. Xu[8], and S. Eldrum[8]

[1] Southwest Research Institute, San Antonio, TX 78238, USA
e-mail: radoslav.bucik@swri.org
[2] Applied Physics Laboratory, Johns Hopkins University, Laurel, MD 20723, USA
[3] Universidad de Alcalá, Space Research Group, 28805 Alcalá de Henares, Spain
[4] Heliophysics Science Division, NASA Goddard Space Flight Center, Greenbelt, MD, USA
[5] George Mason University, Fairfax, VA, USA
[6] Lockheed Martin Advanced Technology Center, Palo Alto, CA 94304, USA
[7] Goddard Planetary Heliophysics Institute, University of Maryland, Baltimore County, Baltimore, MD 21250, USA
[8] Institut für Experimentelle und Angewandte Physik, Christian-Albrechts-Universität zu Kiel, Kiel, Germany
[9] Now at Department of Physics and Astronomy, University of Turku, 20014 Turku, Finland
[10] Leibniz-Institut für Astrophysik Potsdam, 14482 Potsdam, Germany
[11] Now at Paradox Cat GmbH, 80333 München, Germany
[12] Now at German Aerospace Center (DLR), Dept. of Extrasolar Planets and Atmospheres, Berlin, Germany
[13] Now at Univ. Colorado/LASP, Boulder, CO, USA
[14] LESIA, Observatoire de Paris, Université PSL, CNRS, Sorbonne Université, Université de Paris, Paris, France
[15] Radboud Radio Lab, Department of Astrophysics, Radboud University Nijmegen, Nijmegen, The Netherlands

Received 6 April 2021 / Accepted 19 May 2021

ABSTRACT

We report observations of a relatively long period of ^{3}He-rich solar energetic particles (SEPs) measured by Solar Orbiter. The period consists of several well-resolved ion injections. The high-resolution STEREO-A imaging observations reveal that the injections coincide with extreme ultraviolet jets and brightenings near the east limb, not far from the nominal magnetic connection of Solar Orbiter. The jets originated in two adjacent, large, and complex active regions, as observed by the Solar Dynamics Observatory when the regions rotated into the Earth's view. It appears that the sustained ion injections were related to the complex configuration of the sunspot group and the long period of ^{3}He-rich SEPs to the longitudinal extent covered by the group during the analyzed time period.

Key words. acceleration of particles – Sun: abundances – Sun: flares – Sun: particle emission

1. Introduction

^{3}He-rich solar energetic particle (SEP) events show enormous enhancements of rare species, such as the nuclide ^{3}He and ultra-heavy elements, by factors of up to $\sim 10^4$ above the nominal coronal abundances (e.g., Mason 2007; Reames 2021). The events are highly associated (>95%) with type III radio bursts (e.g., Reames & Stone 1986; Nitta et al. 2006), the emission generated by ~10–100 keV outward streaming electrons. Solar sources of ^{3}He-rich SEPs have been associated with extreme ultraviolet (EUV) jets (Bučík 2020, and references therein), suggesting acceleration via magnetic reconnection involving field lines open to interplanetary space (Reames 2002). Progress in understanding ^{3}He-rich SEPs has been hampered by the low intensities and short durations of these events. Solar Orbiter (Müller et al. 2020) will enable unprecedented studies of small-size ^{3}He-rich SEP events, combining in situ and remote-sensing observations close to the Sun.

The first Solar Orbiter ^{3}He-rich SEP events were measured during the spacecraft's first perihelion pass from 0.52 to 0.96 au (Mason et al. 2021) in June–September 2020. Three out of the five discrete events reported by Mason et al. (2021) have a 0.2–2 MeV nucleon^{-1} ^{3}He/^{4}He above 10%, with a maximum ^{3}He/^{4}He of 0.61. In this paper we report a relatively long period of ^{3}He-rich SEPs, spanning almost 7 days in November 2020, observed by Solar Orbiter near 0.9 au. Such a long period may indicate a nearly continuous ^{3}He-rich SEP injection into the interplanetary space (Mason 2007).

2. Observations

The ^{3}He-rich SEPs reported in this paper were measured by the Suprathermal Ion Spectrograph (SIS) of the Energetic Particle Detector (EPD) suite (Rodríguez-Pacheco et al. 2020) aboard Solar Orbiter. The SIS is a time-of-flight mass spectrometer that

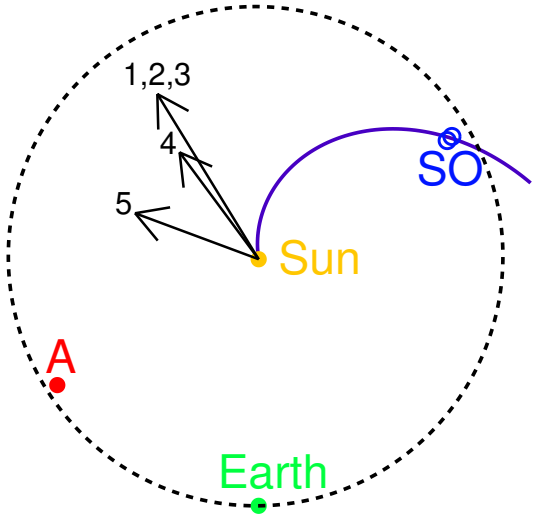

Fig. 1. Ecliptic plane projection of the Solar Orbiter (SO), STEREO-A (A), and the Earth November 17–23, 2020. Two overlapping rings mark Solar Orbiter at the beginning and end of the examined period. The arrows indicate the longitude of the solar source associated with the ion injections. The Parker spiral for the 340 km s^{-1} solar wind speed connecting to Solar Orbiter is shown. The dashed line corresponds to a 1 au orbit.

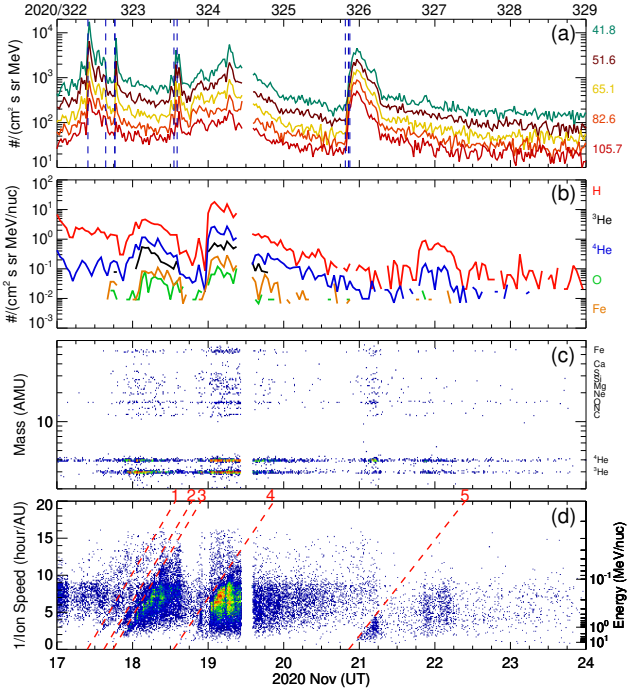

Fig. 2. Solar Orbiter energetic electron and ion measurements during the ^{3}He-rich SEP period. *Panel a*: EPT (41.8–105.7 keV) 30 min electron intensities from the sunward pointing sensor. Dashed vertical lines mark the type III radio bursts listed in Table 1. *Panel b*: SIS 1.0 h H, ^{3}He, ^{4}He, O, and Fe intensities at 0.23–0.32 MeV nucleon^{-1}. *Panel c*: SIS mass spectrogram at 0.4–10 MeV nucleon^{-1}. *Panel d*: SIS 1/speed vs. arrival times of 2–70 AMU ions. Sloped dashed lines approximately mark the ion injections. SIS measurements are from both telescopes and averaged together. The gap around noon on November 19 was caused by EPD being shut down for software maintenance.

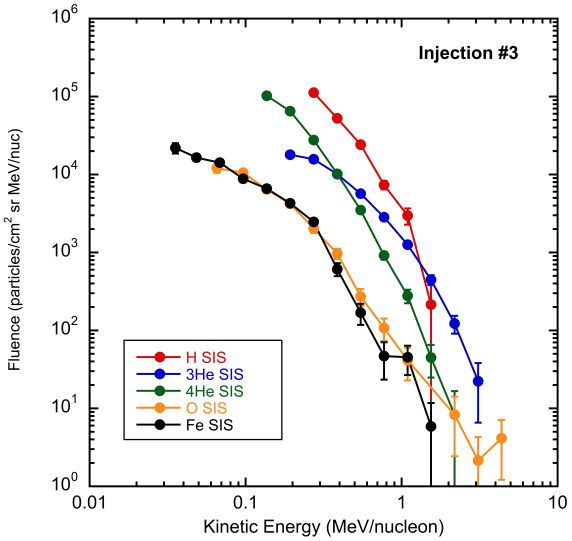

Fig. 3. Fluence spectra for selected species in injection #3.

measures elemental composition from H through ultra-heavy nuclei in the kinetic energy range of ~0.1–10 MeV nucleon^{-1}. The SIS has two telescopes, one pointing 30° (sunward) and the other 160° (anti-sunward) to the west of the spacecraft-Sun line. We also used energetic electron measurements made by the Electron Proton Telescope (EPT) of the EPD, which covers the energy range 20–400 keV, the range in between two other instruments of the EPD suite, STEP and HET. The first year of operations and details of the data products provided by EPD can be found in Wimmer-Schweingruber et al. (2021).

Solar sources of ^{3}He-rich SEPs were examined using high-resolution EUV images from the SECCHI/EUVI instrument (Howard et al. 2008) on STEREO-A. The EUVI provides full-disk images of the Sun with 3″ spatial and 5-minute nominal temporal resolution in four wavelength channels (304, 171, 195, and 284 Å). We used the 195 Å images that have the highest temporal resolution (5.0 and 2.5 minutes) in the examined period. The Extreme-Ultraviolet Imager (EUI; Rochus et al. 2020) on Solar Orbiter provides images with limited spatial and temporal resolution during the aforementioned period. Until November 2021, Solar Orbiter will be in the cruise phase, during which time remote-sensing instruments are only occasionally switched on for calibration. Further, we inspected radio spectrograms for the presence of the associated type III radio bursts. The radio data are provided by the Solar Orbiter Radio and Plasma Waves (RPW; Maksimovic et al. 2020) and the STEREO-A Waves (Bougeret et al. 2008) instruments with a frequency range (<16 MHz) that covers emission generated from about ~2 $R_\odot$ to 1 au. We also made use of full-disk line-of-sight magnetograms obtained from the Helioseismic and Magnetic Imager (HMI; Scherrer et al. 2012) on board the Solar Dynamics Observatory (SDO).

The location of Solar Orbiter and STEREO-A during the investigated period is shown in Fig. 1. Solar Orbiter traveled from 0.93 to 0.91 au; STEREO-A remained at 0.96 au. Both spacecraft were near the ecliptic plane, Solar Orbiter at −6° and STEREO-A at 7° of heliographic latitude. The angular separation between Solar Orbiter and STEREO-A was 180°. The SDO is in orbit around the Earth.

Figure 2 displays Solar Orbiter EPT and SIS measurements from November 17–23, 2020. Figure 2a presents 30 min electron intensities at different energy bins between 41.8 and 105.7 keV. Figure 2b shows hourly averages of the 0.23–0.32 MeV nucleon^{-1} H, ^{3}He, ^{4}He, O, and Fe intensities as

Table 1. Characteristics of the ^{3}He-rich period.

	Ion injection time (UT)	Type III start (UT)	STEREO-A EUVI event Type [a]	STEREO-A EUVI event Location	Separation angle [b](°)	Elec. injection time (UT)	^{3}He/^{4}He [c]	Fe/O [c]
1	322.42 Nov-17 10:05	09:49 [41]	B	E90S22	20	09:20	0.61 ± 0.08	2.00 ± 0.37
2	322.62 Nov-17 14:53	15:28 [20]	B	E90S18	20	...	0.22 ± 0.03	0.63 ± 0.06
3	322.74 Nov-17 17:46	18:20 [12]	J	E90S18	20	18:20	0.90 ± 0.03	0.91 ± 0.01
		18:24 [16]	...	E90S18	20	...	...	...
4	323.54 Nov-18 12:58	13:08 [00]	B	E85S23	25	13:10	0.56 ± 0.01	1.35 ± 0.01
		14:09 [01]	B	E85S23	25	14:07	...	...
5	325.87 Nov-20 20:53	19:34 [26]	B	E48S19	62	19:30	0.32 ± 0.03	0.76 ± 0.03
		20:33 [25]	J	E52S17	58	...	...	...
		21:00 [52]	B	E48S19	62	...	...	...

Notes. See text for more details. [a]B: brightening; J: jet. [b]Between the Solar Orbiter magnetic footpoint longitude on the Sun and the longitude of the EUVI event. [c]0.2–2.0 MeV nucleon^{-1}.

measured by both telescopes of the SIS. Three major increases are seen in the intensity time profiles that start near the end of November 17, near the end of November 18, and around midday on November 21. It is clear that the first two increases are ^{3}He- and Fe-rich. The mass spectrogram in Fig. 2c shows almost continuous ^{3}He presence from the middle of November 17 through the end of November 23 that is ∼6.5 days. The inverse ion-velocity time spectrogram in Fig. 2d shows at least three ion injections contributing to the first increase during the period November 17–18, one injection contributing to the increase November 18–20, and one to the increase on November 21. These injections can be identified based on their characteristic triangular pattern in the inverse speed plots. Figure 3 shows the fluence energy spectra for selected ion species in injection #3, where enhancements in all ion species were observed without the inconvenient data gaps that are present in the case of injection #4. The ^{3}He, O, and Fe show rollovers toward low energies, as has been previously reported in many ^{3}He-rich SEP events (e.g., Mason et al. 2000). The ion fluences for injections #1, #2, and #3 are integrated in swoosh boxes bounded by slanted lines 1 & 2, 2 & 3, and 3 & 4, respectively. For injection #4, the swoosh box is between the slanted line 4 and November 20 19:26 UT and for injection #5 between slanted line 5 and November 22 08:24 UT.

Table 1 lists the characteristics of the ^{3}He-rich period. Column 1 indicates the injection number, and Col. 2 indicates the ion injection time at the Sun (as a day of year and time), estimated via the extrapolation of the dispersive signature of individual ions in the inverted velocity-time spectrogram indicated by the inclined dashed red lines in Fig. 2d. The uncertainty in the injection time estimated by this method is ±45 min (Mason et al. 2000; Wang et al. 2016). Column 3 gives the associated type III radio burst start times as observed by STEREO-A Waves at 16 MHz. The RPW showed an enhanced level of interference at higher frequencies. Multiple type III bursts appear to contribute to injections #3, #4, and #5 (see Fig. 4). To compare with the estimated ion injection times, the square brackets show the minute of the type III burst start times after subtraction of the light travel time (∼8 min). It is unclear if the type III burst at 19:34 UT is associated with injection #5; it occurs too early to be within the ±45 min error of the ion estimated release time. We note that injection #5 is the weakest of all the injections and that the magnetic connection to the site was interrupted early in the event, around 08:00 on November 21 (Fig. 2d), as indicated by the abrupt drop in ion counts at all energies. Therefore, the estimated injection time is only tentative, and the association with the type III burst at 19:34 UT could not be ruled out. Columns 4 and 5 provide the type and location of the associated parent solar eruption, respectively, as seen in the EUVI on STEREO-A, where J indicates a clear EUV jet moving away from the parent active region (AR) and B indicates just a brightening seen in the EUV images without apparent outward movement. We cannot identify the type of EUVI event in 5-minute resolution images for the second type III burst, corresponding to injection #3, that occurred only 4 minutes after the first type III burst. Column 6 indicates a separation angle between the Solar Orbiter magnetic footpoint longitude on the Sun and the longitude of the EUVI event. The magnetic footpoint of Solar Orbiter, based on a simple Parker spiral approximation and assuming a solar wind speed of 340 km s^{-1}, was ∼W70, which corresponds to E110 from the STEREO-A view. The value of 340 km s^{-1} is the median solar wind speed measured by SWEPAM (McComas et al. 1998) on ACE nine days earlier (November 8–12), which corresponds to the solar rotation between the L1 and Solar Orbiter separated by 122°. The Solar Orbiter Solar Wind Analyser (SWA; Owen et al. 2020) data were not available for the examined period. Column 7 shows the electron injection time, estimated from the inverted velocity-time spectrogram (not shown) of 1 min averaged EPD electron data. Columns 8 and 9 provide ^{3}He/^{4}He and Fe/O at 0.2–2.0 MeV nucleon^{-1}.

Figure 4 shows Solar Orbiter and STEREO-A radio spectrograms; we have indicated the type III radio bursts associated with the ion injections. The presence of high frequencies at STEREO-A Waves in all the bursts suggests that the source was not behind the east limb as seen from STEREO-A. The second type III bursts in injections #4 and #5 were weak at Solar Orbiter. During ion injection #3, two small dispersive electron events were detected by EPD with solar injections on November 18 at 10:25 and at 11:45 UT. The later one appears as a small peak in the EPT intensity-time profile at ∼12:00 UT on November 18 (Fig. 2a). Figure 4d shows a type III burst associated with the electron injection at 11:45 UT. The type III burst associated with the electron injection at 10:25 UT is only clearly observed by Solar Orbiter (see Fig. 4d for the low-frequency part, ∼0.05 MHz, between 11:30 and ∼13:00 UT). During ion injection #4, another small dispersive electron event was measured with solar injection on November 19 at 06:00 UT (see Fig. 2a for the peak at ∼07:00 UT on November 19). Figure 4e shows the associated type III radio burst. The type III bursts related to these electron events were accompanied by EUV jets (see Fig. A.3).

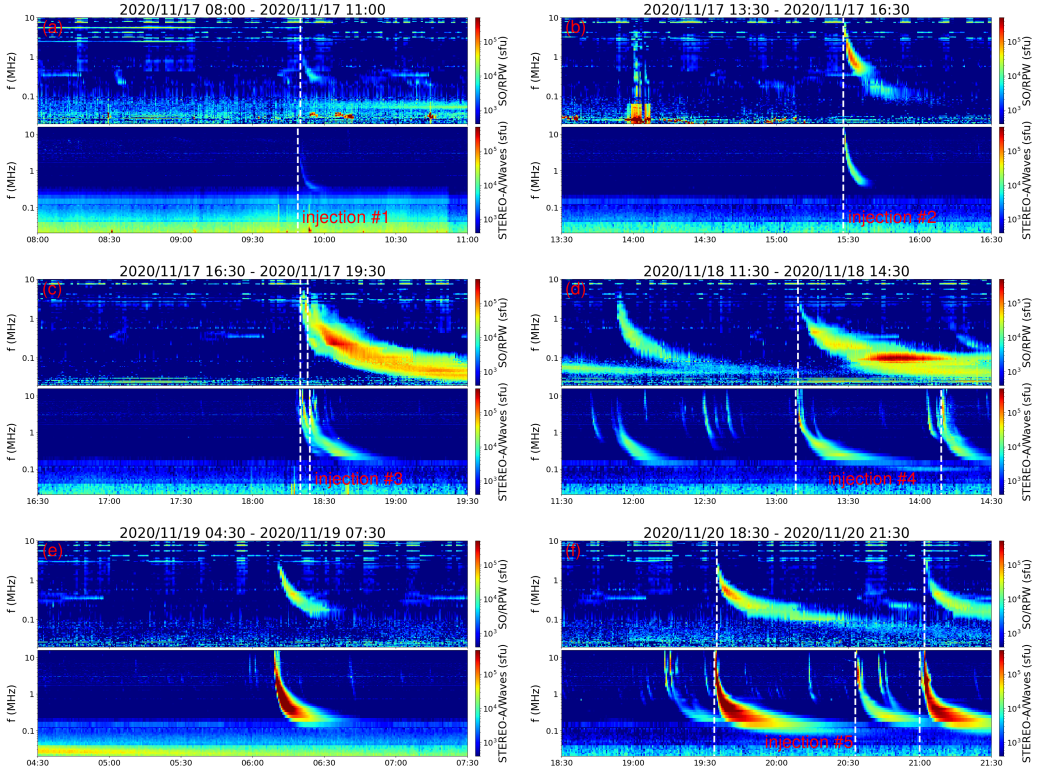

Fig. 4. Solar Orbiter/RPW and STEREO-A Waves radio spectrograms: *panels a–d and f* correspond to ion injections #1 – #4 and #5, respectively, and *panel e* corresponds to an electron event. The vertical dashed lines mark the start times of the type III radio bursts associated with the ion injections.

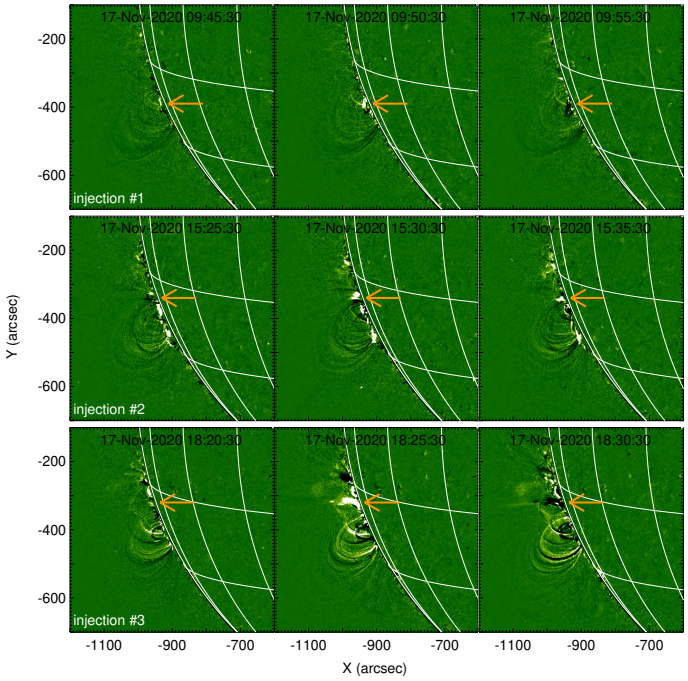

Fig. 5. STEREO-A 195 Å EUV running difference images corresponding to injection #1 (*top row*), #2 (*middle row*), and #3 (*bottom row*). The arrow marks the solar source. The heliographic longitude-latitude grid has a 15° spacing.

To identify solar sources, we inspected full-disk solar images for EUV brightenings as seen by STEREO-A that temporally coincide with the type III radio burst associated with the ion injection. Figure 5 shows the EUV activity around the times of the type III radio burst for injection #1 (top row), #2 (middle row), and #3 (bottom row). We do not see clear jets for injections #1 or #2 in the EUVI images. The EUV images of the solar source for injections #4 and #5 are shown in Appendix A. We note that the SDO was not located at a good position to observe EUV activity related to the origin of these ion injections (Fig. 1). However, for injection #5 the SDO Atmospheric Imaging Assembly (AIA; Lemen et al. 2012) observed the EUV jets, from the region ∼16° behind the east limb, that temporally match all three type III bursts.

On November 17 and 18, the EUI on Solar Orbiter only provided images with 1 hr cadence. On November 19 and 20, there were also higher cadence data, but they either cover only short periods or have a low spatial resolution. The jets and brightenings on November 19 and 20 were missed by EUI.

Figure 6 shows SDO HMI magnetograms on November 24 00:00 UT (left) and November 28 00:00 UT (right). The EUV activity observed by STEREO-A November 17–20 likely originated in two adjacent large ARs, 12785 and 12786, that appeared near the east limb, as viewed from Earth early on November 23. The latitude of the jets and brightenings as indicated in Table 1 and as seen in Figs. 5 and A.1–A.3 matches well with the latitudes of these two ARs. It is particularly well seen in Fig. A.2, where the constellations of bright areas are similar to the positions of these two ARs. Thus, the brightenings in injection #5 can clearly be associated with AR 12785, while the jet occurred between these ARs. AR 12786 shows a complex $\beta\gamma$ magnetic class[1] and sunspot area of 1000 millionths of the solar hemisphere (MH) November 25–26. AR 12785 has a

[1] $\beta\gamma$ denotes a bipolar sunspot group with no clearly marked line separating spots of opposite polarity; β indicates a bipolar sunspot group.

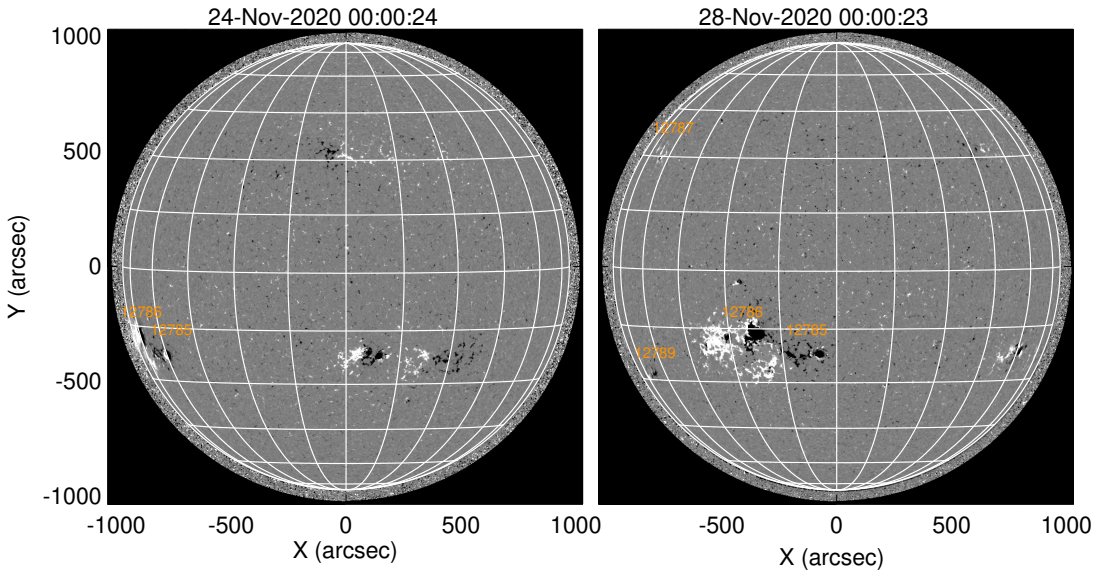

Fig. 6. SDO HMI line-of-sight magnetograms (scaled to ±100 G). The numbers mark the NOAA ARs of interest. The heliographic longitude-latitude grid has a 15° spacing.

simple β magnetic class and sunspot area of 140 MH (November 23–24). This information is provided by the Solar Region Summary (ftp.swpc.noaa.gov/pub/warehouse/2020/SRS). The magnetic complexity of the ARs decreased after they crossed the central meridian (as observed by SDO) on November 29–30. These ARs were seen by STEREO-A in EUV for the first time on November 19 (they were not reported in the previous rotation), and therefore we do not know what their properties were on November 17. As STEREO-A does not have a magnetograph, the magnetic class and area of the ARs were unknown when the examined activity was occurring. Also marked are two small ARs, 12787 and 12789 (Fig. 6 right), that could be located close to the Solar Orbiter nominal magnetic footpoint longitude. If these regions were in the hidden hemisphere, we cannot confirm or rule out that there was some simultaneous activity occurring in them as well. However, it is improbable that these regions dominated the observed long period of ^{3}He-rich SEPs as all type III radio bursts temporally coincide with jets or brightenings in AR 12786 and AR 12785.

3. Discussion and conclusion

The relatively long period of ^{3}He-rich SEPs observed by Solar Orbiter is related to the recurrent activity (brightening and jets) in a large and complex group of sunspots in two adjacent ARs. Recurrent ^{3}He-rich SEP events have been found to originate from ARs at the boundary of low-latitude coronal holes (e.g., Wang et al. 2006; Bučík et al. 2014). There are only a few reports of ^{3}He-rich SEPs associated with sunspot jets (Nitta et al. 2008; Bučík et al. 2018), and none of them report recurrent ion injection. The configuration with two large and complex nearby ARs may be favorable for the recurrent particle injections in the sense that there may be a long-lived interaction between the negative polarity of one AR and the positive polarity of the neighboring AR, leading to the magnetic reconnection. Furthermore, these two ARs produce a longitudinally extended source (~40°) in which spacecraft may be magnetically connected for a long period as the Sun rotates. We note that this extended region is rotating away from Solar Orbiter, and as such the magnetic connection is presumably weakening with time.

Kocharov et al. (2008) studied extended periods of ^{3}He-rich SEPs, and most showed no dispersive onset. The authors suggested that the temporal confinement of ions in the solar wind structures is an essential factor in the occurrence of such periods. Chen et al. (2015) reported two relatively long, 4-day, periods of ^{3}He-rich SEPs that were produced by recurring injections originating from dispersed sunspots in plage regions. While Chen et al. (2015) identified two injections per period, we report at least five ion injections responsible for a long period. There might have been other unresolved ion injections during the decay phase of the first and second ion intensity increases.

The recurrent production of ^{3}He-rich SEPs appears to occur in different magnetic environments that include plages, coronal holes, and sunspots and may be the result of a common process. Further studies may confirm whether complex and longitudinally extended sunspot groups are responsible for longer ^{3}He-rich SEP periods compared to simple and small-size sources.

Acknowledgements. The Suprathermal Ion Spectrograph (SIS) is a European facility instrument funded by ESA. The SIS instrument was constructed by the JHU/Applied Physics Lab. and CAU Kiel. We thank the many individuals at ESA and within the Energetic Particle Detector team for their support in its development. Post launch operation of SIS at APL is funded by NASA contract NNN06AA01C, and we thank NASA headquarters and the NASA/GSFC Solar Orbiter project office for their continuing support. The UAH team acknowledges the financial support by the Spanish Ministerio de Ciencia, Innovación y Universidades FEDER/MCIU/AEI Projects ESP2017-88436-R and PID2019-104863RB- I00/AEI/10.13039/501100011033. The CAU Kiel team thanks the German Federal Ministry for Economic Affairs and Energy and the German Space Agency (Deutsches Zentrum für Luft- und Raumfahrt, e.V., (DLR)) for their unwavering support under grant numbers 50OT0901, 50OT1202, 50OT1702, and 50OT2002; and ESA for supporting the build of SIS under contract number SOL.ASTR.CON.00004, and the University of Kiel and the Land Schleswig-Holstein for their support of SIS. R. Bučík is supported in part by NASA grant 80NSSC19K0079. F. Carcaboso acknowledges the financial support by the Spanish MINECO-FPI-2016 predoctoral grant with FSE. V. Krupař acknowledges the support by NASA under grants 18-2HSWO2182-0010 and 19-HSR-192-0143. L. Balmaceda acknowledges the support from the NASA program NNH17ZDA001N-LWS (Awards Nr. 80NSSC19K1261 and 80NSSC19K1235).

References

Bougeret, J. L., Goetz, K., Kaiser, M. L., et al. 2008, Space Sci. Rev., 136, 487
Bučík, R. 2020, Space Sci. Rev., 216, 24
Bučík, R., Innes, D. E., Mall, U., et al. 2014, ApJ, 786, 71
Bučík, R., Wiedenbeck, M. E., Mason, G. M., et al. 2018, ApJ, 869, L21
Chen, N.-H., Bučík, R., Innes, D. E., & Mason, G. M. 2015, A&A, 580, A16
Howard, R. A., Moses, J. D., Vourlidas, A., et al. 2008, Space Sci. Rev., 136, 67
Kocharov, L., Laivola, J., Mason, G. M., Didkovsky, L., & Judge, D. L. 2008, ApJS, 176, 497
Lemen, J. R., Title, A. M., Akin, D. J., et al. 2012, Sol. Phys., 275, 17
Maksimovic, M., Bale, S. D., Chust, T., et al. 2020, A&A, 642, A12
Mason, G. M. 2007, Space Sci. Rev., 130, 231
Mason, G. M., Dwyer, J. R., & Mazur, J. E. 2000, ApJ, 545, L157
Mason, G. M., Ho, G. C., Allen, R. C., et al. 2021, A&A, 656, L1 (SO Cruise Phase SI)
McComas, D. J., Bame, S. J., Barker, P., et al. 1998, Space Sci. Rev., 86, 563
Müller, D., St. Cyr, O. C., Zouganelis, I., et al. 2020, A&A, 642, A1
Nitta, N. V., Reames, D. V., De Rosa, M. L., et al. 2006, ApJ, 650, 438
Nitta, N. V., Mason, G. M., Wiedenbeck, M. E., et al. 2008, ApJ, 675, L125
Owen, C. J., Bruno, R., Livi, S., et al. 2020, A&A, 642, A16
Reames, D. V. 2002, ApJ, 571, L63
Reames, D. V. 2021, Solar Energetic Particles (Cham.: Springer), 978
Reames, D. V., & Stone, R. G. 1986, ApJ, 308, 902
Rochus, P., Auchère, F., Berghmans, D., et al. 2020, A&A, 642, A8
Rodríguez-Pacheco, J., Wimmer-Schweingruber, R. F., Mason, G. M., et al. 2020, A&A, 642, A7
Scherrer, P. H., Schou, J., Bush, R. I., et al. 2012, Sol. Phys., 275, 207
Wang, L., Krucker, S., Mason, G. M., Lin, R. P., & Li, G. 2016, A&A, 585, A119
Wang, Y. M., Pick, M., & Mason, G. M. 2006, ApJ, 639, 495
Wimmer-Schweingruber, R. F., Janitzek, N. P., Pacheco, D., et al. 2021, A&A, 656, A22 (SO Cruise Phase SI)

Appendix A: EUV images of the solar sources

The solar sources associated with injections #4 and #5 and the electron events that occurred during the decay phase of the first and second ion intensity increases are shown in Figs. A.1–A.3, respectively.

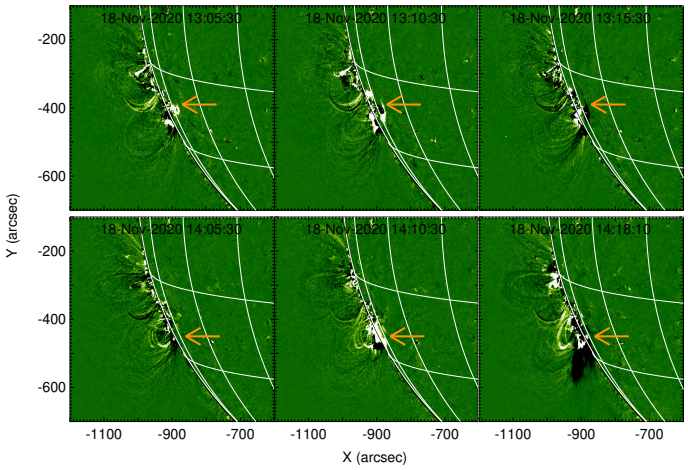

Fig. A.1. Same as Fig. 5 but for injection #4. *Top and bottom rows*: correspond, respectively, to the first and second type III bursts.

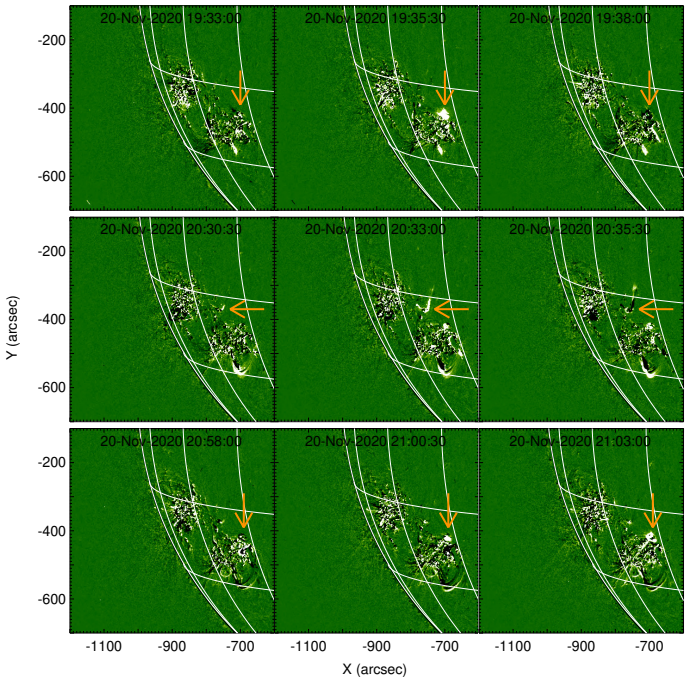

Fig. A.2. Same as Fig. 5 but for injection #5. *Top, middle, and bottom rows*: correspond, respectively, to the first, second, and third type III bursts.

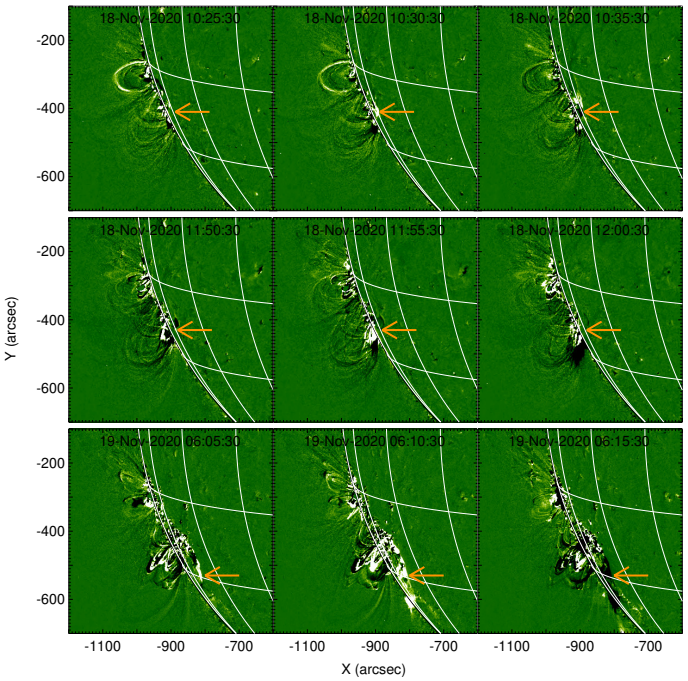

Fig. A.3. Same as Fig. 5 but for the electron events that occurred during the decay phase of the first (*top and middle panels*) and second ion intensity increases (*bottom panel*).